ELSEVIER

Materials Science and Engineering A344 (2003) 113–124

MATERIALS SCIENCE & ENGINEERING A

www.elsevier.com/locate/msea

Modeling the strengthening response to aging process of heat-treatable aluminum alloys containing plate/disc- or rod/needle-shaped precipitates

G. Liu [a], G.J. Zhang [a], X.D. Ding [a], J. Sun [a,*], K.H. Chen [b]

[a] *State Key Laboratory for Mechanical Behavior of Materials, School of Material Science and Engineering, Xi'an Jiaotong University, Xi'an 710049, China*

[b] *State Key Laboratory for Powder Metallurgy, The University Of Southern Central China, Changsha, China*

Received 1 February 2002; received in revised form 22 May 2002

Abstract

For the heat-treatable aluminum alloys containing plate or rod/needle-shaped precipitates, a previous model was modified to present quantitative relationships between the yield strengths of the alloys and the sizes, volume percentages of precipitates, related to aging temperature and aging time as well as alloy compositions, while the strengthening of the precipitates was coupled with the whole evolution process, i.e. nucleation, growth and coarsening, of the precipitates. It was found that the aging yield strengths have been well predicted by the model for a series of aged Al–Cu binary alloys, 6061 alloys and Al–Zn–Mg alloys. It was also experimentally proved that the model was suitable to evaluate the aging strengthening of the precipitates for an Al–Cu–Mg alloy and an Al–Mg–Si alloy. Furthermore, a detailed discussion has been made to the variation of aspect ratio of precipitates, relative to its strengthening response, with aging parameters and alloy compositions.
© 2002 Published by Elsevier Science B.V.

Keywords: Aluminum alloys; Aging; Plate/disc- or rod/needle-shaped precipitates; Yield strength modeling; Aspect ratio

1. Introduction

The low density combined with high strength have made aluminum alloys the primary material of choice for application such as in aircraft, where specific strength (strength-to-weight ratio) is a major design consideration. The significant contribution to the high strength of heat-treatable aluminum alloys is due to the precipitation of excess alloying elements from supersaturated solid solution to form fine second phase particles that will act as obstacles to moving dislocations. Composition, manufacture technology, and heat treatment all affect precipitation evolution therefore determine the strengthening response. Understanding well, especially in a quantitative manner, how these controlling factors exert their influences on microstructures further on engineering mechanical behaviors is very rewarding because the ability to predict and control the desired microstructures is central for developing advanced aluminum alloys that could achieve the progressively desired level of performance. Thus this area of researches has received a great deal attention resulting in many theoretical models together with derived expressions suggested to display the dependence of microstructures on controlling factors and/or the dependence of engineering yield strength on microstructures [1–20].

Among those models, the earlier ones were exclusively focused either on the mere physical aspects of precipitation process [1–6], such as thermodynamics and kinetics for precipitation process, or on the mere strengthening aspects of precipitated second phases [7–12], such as the effects of the characteristics, sizes and shapes of precipitates on strengthening. Nothing had been taken into account about bridging this two aspects until a pioneer model was suggested in which a first attempt was made to establish mathematical relationships between the

* Corresponding author. Tel.: +86-29-2667143; fax: +86-29-2663453

E-mail address: junsun@mail.xjtu.edu.cn (J. Sun).

0921-5093/02/$ - see front matter © 2002 Published by Elsevier Science B.V.
PII: S0921-5093(02)00398-2

process variables (alloy composition, and heat-treatment temperature and time) and the yield strength or hardness for aged aluminum alloys [13,14]. The success of this model was assessed in application to describe the changes of yield strength of 2000 and 6000 series aluminum alloys due to age hardening. But this model revealed less in the evolvement of precipitates from the viewpoint of thermodynamics and kinetics. Subsequently, an overall process model having completely analytical sense was brought to success [15,16], in which the nucleation, growth and coarsening of precipitate together with structural strengthening were integrally simulated and the predicted values of this model were perfectly in agreement with experimental results. Along this line, deep-going work has been carried out widely and fruitfully and it seems that these scientific principles should be applied to aluminum alloys by replacing empiricism in the near future [17–20].

However, all the strengthening precipitates assumed in the aforementioned advanced models were simply treated as be in spherical shape. This was failed in accurately representing the truth because practical precipitates in heat-treatable aluminum alloys are usually plate-like or rod (needle)-like shape, just like the θ′-Al_2Cu in Al–Cu alloy, the β′-Mg_2Si in AA6061 and the η′-$MgZn_2$ in AA7075. The reason for this simplification is that plate (rod)-shaped precipitates are difficult to be precisely simulated in its interaction with dislocations hence in its strengthening action because of their complicated morphology and multidirectional orientation in spite of several simple model having been proposed earlier [21–23]. Fortunately, this hindrance was subtly overcome by ad hoc fitted expressions that were obtained from simulating a dislocation–slip process on one slip plane through randomly distributed particles which were oriented in the same habit directions as the actual cases by using computer programs [24–26]. This notwithstanding, no attention has been paid on studying the integral evolution, including both the microstructure evolution and the mechanical behavior evolution, of age hardening of aluminum alloys containing plate (rod/needle)-shaped precipitates with the process variables (alloy composition, and heat-treatment temperature and time) up to now. In present work we will make a trial on this modeling and attempt to validate it by experimentally examining the evolvements of precipitates and the variation of yield strength in an aged Al–Cu–Mg alloy and in an aged Al–Mg–Si alloy, respectively.

2. Modification and evaluation of model

2.1. Modification of model

Similar to analogous models, a single population of precipitates is assumed existing for simplicity. If these plate-shaped precipitates are considered as unshearable regardless of how lager their dimensions are, so moving dislocations have to bow out and bypass between adjacent plate-shaped precipitates in order to slip further, which introduces an increment in the yield strength [26]:

$$\Delta\sigma = 0.13MG\frac{b}{2\sqrt{rh}} \times \left[f_v^{1/2} + 0.75\left(\frac{r}{h}\right)^{1/2} f_v + 0.14\left(\frac{r}{h}\right) f_v^{3/2}\right] \ln\left(\frac{0.158r}{r_0}\right)$$

(for {1 0 0} plate-shaped precipitates) (1a)

$$\sigma = 0.12MG\frac{b}{2\sqrt{rh}} \times \left[f_v^{1/2} + 0.70\left(\frac{r}{h}\right)^{1/2} f_v + 0.12\left(\frac{r}{h}\right) f_v^{1/2}\right] \ln\left(\frac{0.158r}{r_0}\right)$$

(for {1 1 1} plate-shaped precipitates (1b)

where M denotes the Taylor factor, G the shear modulus, b the magnitude of the Burgers vector, r_0 the inner cut-off radius for the calculation of the dislocation line tension, and r, h and f_v are the radius of habit plane, the half-thickness of peripheral plane and volume fraction of plate-shaped precipitates, respectively. Although Eq. (1a) or Eq. (1b) has been used to successfully predict the increments of yield strength in some aged aluminum alloys, where the dimensions and volume fractions of precipitates were given individually [25,26], it has not been proven to be suitable for predicting the continuous strengthening responses of the precipitates during the whole aging process. When the Eq. (1a) or Eq. (1b) is used, the parameters of r, h and f_v will be varied with aging time, t, according to the HHC theory [5–7], standard Becker–Doring law [27,28] and some other relevant experimental results [29–31]:

$$r = \frac{2}{3}\sqrt{A^2\beta Dt} \quad (2a)$$

$$h = \frac{2}{3}\sqrt{\beta Dt} \quad (2b)$$

$$f_v = \frac{2\pi r^3}{A} A_0 N_0 Z\beta^* \exp\left(\frac{-\Delta G^*}{RT}\right) t \quad (2c)$$

where A is the aspect ratio of precipitates, β is a dimensionless growth parameter which is in proportion to the supersaturation $\Omega(=(C_0 - C_e)/(C_p - C_e))$ and can be valued by the formula of $\beta = \Omega/pA$ with p being a factor [32], where the factor of 2/3 will be taken in Eq. (2) to reflect the effect of continuous precipitation. A_0 is the Avogadro number, N_0 is the number of mole by unit volume ($=1/v_{at}$), Z is the Zeldovich's factor (≈ 0.05 [33]), T is the aging temperature, ΔG^* is the critical activation energy for precipitation, the parameter of β^*

is obtained by

$$\beta^* = 4\pi(r^*)^2 DC_0/a^4 \quad (3)$$

with D being the diffusion coefficient of solute atom in solvent, a the lattice parameter of precipitate, and the critical radius for precipitates, r^*, being obtained by

$$r^* = 2\gamma/\Delta F_v \quad (4)$$

where γ is the precipitate-matrix interfacial energy and ΔF_v is the driving force per mole of solute atom to precipitate from supersaturated solid solution:

$$\Delta F_v = \frac{RT}{v_{at}}\left[C_p \ln\left(\frac{C_0}{C_e}\right) + (1 - C_p)\ln\left(\frac{1 - C_0}{1 - C_e}\right)\right] \quad (5)$$

where v_{at} is the molar volume of precipitate, C_0, C_e, and C_p are mean solute concentrations by atom percentage in matrix, equilibrium precipitate-matrix interface, and precipitates, respectively. It is clearly seen from the aforementioned equations that, for any given aluminum alloy of certain compositions, aged at given temperatures, the unknown and hence key parameters to predict the continuous strengthening effects with aging time are ΔG^* and A. Although the two parameters are influenced directly by many factors therefore are not valued readily, in this model they could be calibrated from two principles. Firstly, it is assumed here that the growth stage of precipitates is terminated once the excess solute atoms are exhausted totally, i.e. $f_v \times C_p = C_0 - C_e$. At the peak-aging moment, defining $t = t_m$, $r = r_m$, then the maximum volume fraction of precipitates is obtained:

$$f_m = \frac{2\pi r_m^3}{A} A_0 N_0 Z\beta^* \exp\left(\frac{-\Delta G^*}{RT}\right) t_m = (C_0 - C_e)/C_p \quad (6)$$

Secondly, as a characteristic parameter for heat-treatable aluminum alloys, the total yield strength at peak-aging condition, σ_m, obtained by putting the increment in the aging strengthening of the precipitates, $\Delta\sigma_m$, together with the intrinsic yield strength, σ_i,

$$\sigma_m = \sigma_i + \Delta\sigma_m, \quad (7)$$

must be ensured to be equal to the measured value of σ_m^{mea}:

$$\sigma_m = \sigma_m^{mea} \quad (8)$$

Combining Eq. (8) with Eq. (6), because all the other parameters are either constants or determined previously, the values of ΔG^* and A can be calibrated by using experimentally measured t_m and σ_{max}.

2.2. Evaluation of model

2.2.1. For aged binary Al–Cu alloys

The most detailed data set available to us is that of Hardy [34] for the aging of binary Al–Cu alloys containing 2, 3, 3.5, 4, and 4.5 wt.% copper at five temperatures between 403 and 513 K (noting: yield strength is approximately three times the Vickers Microhardness for aluminum alloys [15,16]). Therefore we assessed the modified model by applying it to predict the age-hardening of binary Al–Cu alloys by treating unshearable {1 0 0} plate-shaped θ′ phase as the only kind of precipitates. Firstly, substituting certain values of some physical and mechanical parameters for Al–Cu alloys and θ′ precipitate as listed in Table 1 together with t_m and σ_{max} determined by Hardy [34] into Eq. (6) and Eq. (8). And ΔG^* and A for binary Al–Cu alloys with various compositions at different aging temperatures were calibrated out and tabulated in Table 2 and depicted later in Fig. 12, respectively. The values of calibrated A is very close to the previous experimental or theoretical results of 12–40 [45–48]. Secondly, ΔG^* and A, along with other variant or constant parameters, were reused back into Eq. (1a) to indicate the variation of yield strength with aging temperature and aging time, which were then drawn as curves and compared with experimental results as in Fig. 2. It is displayed clearly in Fig. 2 that the modified model perfectly predicts the yield strength of aged Al–Cu alloys at the overaged stage despite of somewhat underestimating the values at the underaged stage, which attests the reliability of this model to a large extent. For the underestimation in yield strengths, it is attributed to the underestimation in volume fraction of precipitates as discussed in detail in Section 4.

2.2.2. For aged 6061 alloy

The major strengthening precipitate in AA6061 is the second phase of rod-shaped β′. For the shape of rod as illustrated in Fig. 1b, it is reasonable to look it as a lengthened plate only with the A changed to be the mean ratio of half length (l) to radius (r), i.e. $A = l/r$. Correspondingly, the growth expression of rod-shaped precipitates is rewriten from Eq. (2a) and Eq. (2b) as:

$$r = \frac{2}{3}\sqrt{\beta Dt} \quad (9a)$$

Table 1
Summary of input data used for aged Al–Cu alloy and θ' precipitate

Parameters	Expression or value	References
γ (J m^{-2})	0.15	[35]
v_{at} ($\times 10^{-5}$ m^3 mol^{-1})	2.9	[36]
a (nm)	0.404	[37]
b (nm)	0.286	[38]
C_e (at.%)	13.176 exp(–4.168 $\times 10^4/RT$)	[39–41]
D (m^2 s^{-1})	6.0 $\times 10^6$ exp(–119691/RT)	[42]
M	3.1	[43]
G (GPa)	28	[38]
r_0 (nm)	0.572	[44]

Table 2
Presently calibrated critical nucleation-energy-barriers and formerly determined intrinsic yield strengths [13,14] for aged Al–Cu alloys

Cu content (wt.%)	Aging temperature (K)	ΔG^* (kJ mol^{-1})	σ_i (MPa)
2	403	92.57	118.5
	438	108.65	
	463	117.08	
	493	129.90	
3	438	100.36	151.5
	463	108.63	
	493	124.55	
3.5	438	96.49	168.0
	463	107.07	
	493	114.68	
4	438	90.4941	189.0
	463	102.37	
	493	113.51	
	513	118.33	
4.5	438	87.73	207.0
	463	101.36	
	493	105.80	

$$l = \frac{2}{3}\sqrt{A^2\beta Dt} \tag{9b}$$

Besides, the parameter of r in the term of $\ln(0.158r/r_0)$ of Eq. (1a) or Eq. (1b) needs to be replaced by the parameter of l. And then the modified model can be applied to predict the yield strength response to aged aluminum alloys containing rod-shaped precipitates.

A series of aging curves have been given for AA6061 (composition: 0.6% Si, 1% Mg, 0.25% Cu, and 0.25% Cr by weight percentage) aged at different temperatures with detailed data for peak-aging time and yield strength being presented [13,49]. For simplicity, in current modeling the existence of elements of Cu and Cr are neglected and the atoms of Mg and Si are supposed to form Mg_2Si according to stoichiometry. It then comes to the comparison of simulated curves with the measured counterparts as depicted in Fig. 3 by following the same treatment procedure described in Section 2.2.1 and adopting the physical parameters for 6061 and β′ precipitate in Table 3 (Mg being assumed to be the less mobile constituent atom in the β′ precipitate). Just contrary to the cases for Al–Cu alloy, the predicted values for AA6061 are quite a few less than the true yield strengths at the overaged stage while fit better with the true ones at the underaged stage. But a common trend is shared by the two cases, which is that the more is the aging temperature, the less is discrepancy between the predicted yield strengths and the measured ones. And some relevant explanations will be elucidated in the later discussion section.

The calibrated ΔG^* of ~ 60 kJ mol^{-1} and A of ~ 50 for AA6061 are both some larger than corresponding previously suggested values (~ 19 kJ mol^{-1} and ~ 25) [50,54], but they are on the same order of magnitude as their corresponding ones, respectively. Anyway, it is approved that the modified model is feasible for aluminum alloys containing rod (needle)-shaped-precipitate.

2.2.3. For aged Al–Zn–Mg alloy

The most important strengthening precipitate in aged Al–Zn–Mg alloys, η′, has been reported to exhibit {1 1 1} plate-shaped shapes [30,55,56]. Hence Eq. (1b) can be applied to predict the yield strength of aged Al–Zn–Mg alloys.

The aging curves for several groups of contrarily treated Al–6.1 wt.% Zn–2.35 wt.% Mg alloy, including water quenched vs air quenched and with 10% vs without predeformation before aging, have been explicitly presented in earlier investigations [13,14,57]. It is surprising that the modified model, being input the values in Table 4, presents well agreeable results with the actual yield strengths for all the three differently treated Al–Zn–Mg alloys (Fig. 4). In common sense, the yield strength of 7000 series alloys is the most difficult to be modeled because a more complicated precipitation sequence involving many stages is existed in these alloys. However, the current model is found to be very suitable for 7000 series alloys.

Although three kinds of heat-treatable aluminum alloys have been used to satisfactorily verify the validity of the model modified presently, all the measured values were come from others' experiments and many relevant microcosmic evolutions of precipitates were not shown in the publications. This brings about some disadvantage in explaining the discrepancy between predicted yield strength and measured values by the analysis to microstructural changes. Therefore, it is necessary to carry out purposeful experiments to identify the difference among the predicted and measured.

3. Experimental procedures

Two kinds of aluminum alloys, supplied in the form of extruded rod by Research laboratory of Xi'an air craft industry LTD., were used in present experiment to validate this model. The one is Al–Cu–Mg alloy with chemical composition being Cu: 4.62%, Mg: 0.65%, Mn: 0.22%, Si, Fe, Zn <0.30%, Al: balance (weight percentage), the other one is Al–Mg–Si alloy having the chemical composition in weight percentage of Mg: 1.12%. Si: 0.57%, Cu: 0.25%, Cr: 0.22%, Al: balance. The Al–Cu–Mg alloys were solution-treated at 766 K for 2 h followed by water quench and subsequently were aged at 513 K for various times from 0.25 h to 10 days. The Al–Mg–Si alloys were solution-treated at 703 K for half-hour followed by water quench and then were aged

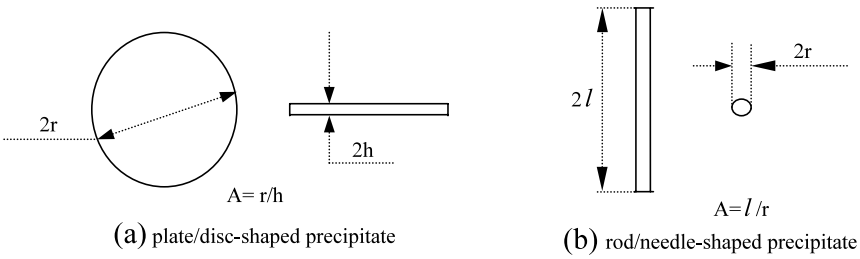

Fig. 1. The morphology of (a) plate/disc or (b) rod/needle-shaped precipitate and definition of parameters used in this paper.

at 463 K for a series of time from 0.25 h to 10 days. At room temperature, the dog-bone shaped tensile specimens from both alloys, having a gage size of 6 mm in diameter and 40 mm in length, were served in the tensile test at a constant strain rate of 5×10^{-4} s^{-1}on a servohydraulic Instron-1346 testing machine. The yield stress was determined as the 0.2% offset.

Thin foils for microstructural characterizations in transition electron microscope (TEM) were prepared by mechanical thinning with SiC paper to 100 μm

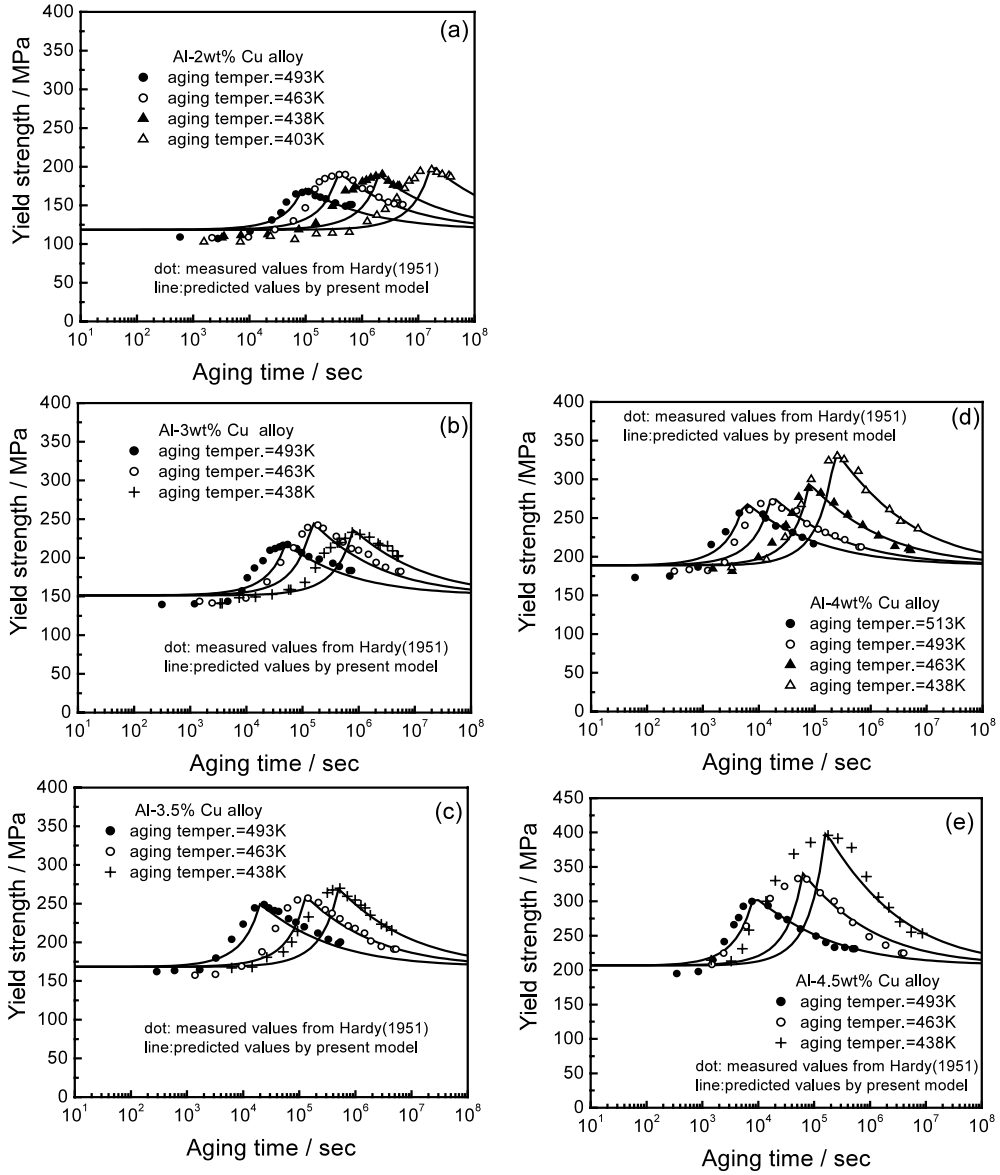

Fig. 2. Data from Ref. [34] (scatter dots) compared with the presently modeled lines for the yield strength of Al–Cu binary alloys (a) Al–2 wt.% Cu alloy; (b) Al–3 wt.% Cu alloy; (c) Al–3.5 wt.% Cu alloy; (d) Al–4 wt.% Cu alloy; and (e) Al–4.5 wt.% Cu alloy.

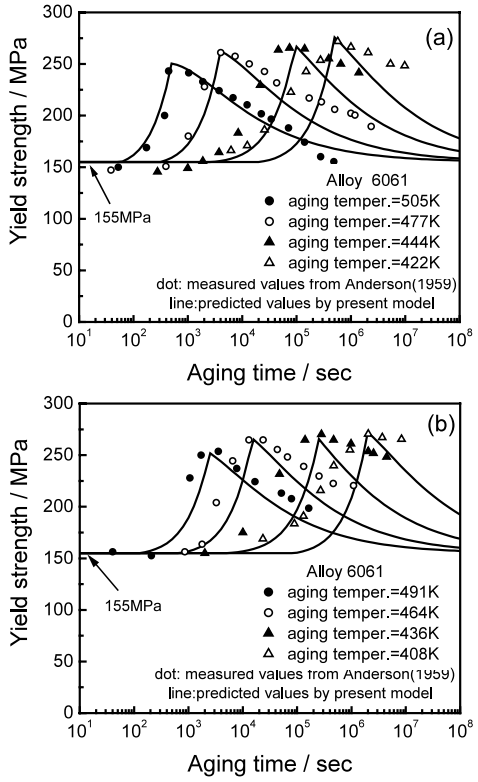

Fig. 3. Data from Ref. [49] (scattered dots) compared with the presently modeled lines for yield strength of 6061 alloy (spread over two figures for clearly seeing).

Table 3
Summary of input data used for aged 6061 alloy and β′ precipitate

Parameters	Expression or value	References
γ (J m^{-2})	0.26	[50]
v_{at} ($\times 10^{-5}$m^3 mol^{-1})	7.62	[50]
C_e (wt.%)	$(C_e^{Mg})^2 C_e^{Si} = \exp\left(\frac{112 \times T - 9.4 \times 10^4}{RT}\right)$	
	[a] $(C_e^{Si} = C_o^{Si}) - \frac{1}{2}(C_o^{Mg} - C_e^{Mg})$	[50–52]
D (m^2 s^{-1})	$4.4 \times 10^{-4}\exp(-140300/RT)$	[53]

[a] C^i_0, nominal solute concentration of element i in matrix; C^i_e, equilibrium solute concentration of element i in particle/matrix interface.

followed by electropolishing with an applied potential of 15 V in a 3:1 methanol–nitric acid solution cooled to −25 °C (248 K). Prepared samples were rinsed twice in methanol, dried, and examined immediately in a JEOL Ltd. JEM-200CX TEM at 100 kV.

Table 4
Summary of input data used for an Al–Zn–Mg alloy aged at 433 K [15,16] and η′ precipitate

Parameters	Expression or value	References
γ (J m^{-2})	0.30	[15,16]
C_e (at.%)	1.1	[15,16]
D (m^2 s^{-1})	5×10^{-20}	[15,16]

Accompanying with TEM observations, the geometrical parameters of precipitates were determined. The dimensions of precipitates were obtained with populations of about 1500 precipitates seen edge-on and the aspect ratio was therefore derived from dividing of thicker dimension by thinner dimension. As the thicker dimension of precipitates, i.e. the diameter of plate-shaped precipitates or the half length of rod/needle-shaped precipitates, is of the same order and sometimes greater than the thickness of the thin foil, a correction is necessary to determine the real dimension from the observed one [58] and the volume fraction of oriented precipitates in a thin-foil projection (corrected for truncation and overlap) was determined by [59]

$$f_v = \left(\frac{-2\pi r}{\pi r + 4t}\right)\ln(1 - A_A) \quad (10)$$

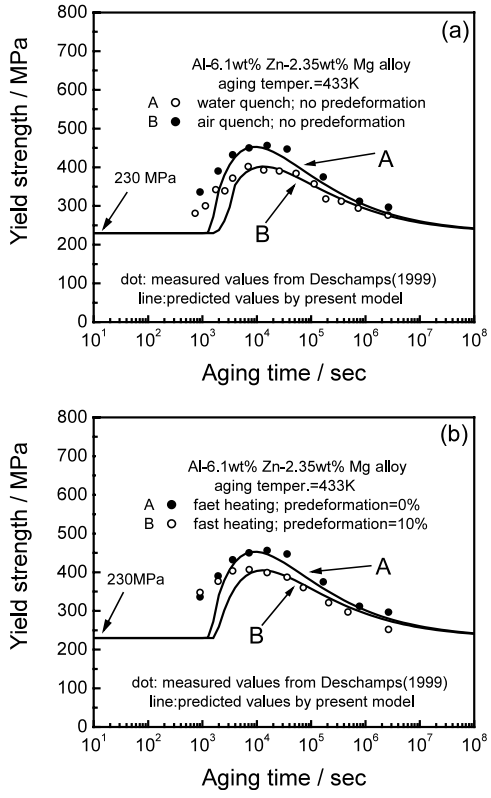

Fig. 4. Data from Refs. [15,16] (scatter dots) compared with the presently modeled lines for yield strength of an Al–Zn–Mg alloy (spread over two figures for clearly seeing).

where r is the radius of plate-shaped precipitates (replaced by l for rod-shaped precipitates), t is the foil thickness, and A_A is the projected area fraction of precipitates, determined by the point count method. The foil thickness was easily obtained by utilizing a grain boundary fringes technique [60].

4. Results

4.1. The dimension evolution of precipitates

The content of Cu and Mg in present Al–Cu–Mg alloy is 4.62 wt.% and 0.65 wt.%, respectively. It has been claimed that in Al–Cu–Mg alloy the dominant precipitates are the $\theta' - Al_2Cu$ phases and the $S' - Al_2CuMg$ phases are very less if the ratio between the content of Cu and Mg is larger than 8 [61]. Hence the major precipitates in present Al–Cu–Mg alloy are θ′ precipitates, and the values of parameters used in Section 2.2.1 are still operative in modeling the evolution of both the dimensions of precipitates and the yield strength here.

The dimension evolutions of precipitates in aging process are typically revealed in Fig. 5 and Fig. 6 for the present two alloys, respectively, and Fig. 7 shows the variation of radius of plate-shaped precipitates (for Al–Cu–Mg alloys) and half-length of rod-shaped precipitates (Al–Mg–Si alloys) with aging time by the experimentally measured values compared with the predicted lines. It is seen that the predicted values are little larger than the measured ones at the underaged stage and the forepart of overaged stage. But after the aging time was elongated, the actual radius or half-length of precipitates gets a very low growth rate nearly as keeping unchanged. Boyd and Nicholson [47,48] have found that at the beginning of aging the growth of θ′ precipitates followed a $t^{1/3}$ law. However, in present experiments, despite some underestimation in simulation, the growth of diameter of θ′ precipitates is prone to follow the $t^{1/2}$ law. Moreover, the growth rate of thinner dimension of precipitates is much less at the underaged stage and the forepart of overaged stage, as discussed latter, it is concluded then that the growth of precipitates is interface-reaction dominant even the growth mechanism is volume reaction.

4.2. The morphological evolution of precipitates

From Fig. 5 and Fig. 6, it could be seen that the aspect ratio of precipitates is as well changing during the aging process in the present two aluminum alloys. As reflected in Fig. 8, the variation trend of measured aspect ratio is that initially the aspect ratio increase monotonously to a maximum value and whereafter decrease monotonously, similar to the conclusions of Merle et al. [62,63] and Sankaran et al. [64,65]. This is also easy to be understood qualitatively because the potential for growth of habit plane of precipitates is gradually exerted to the most extent. Once this potential being exhausted after prolonged aging, the ability of growth of inherent plane is then coming to cut a conspicuous figure. Merle et al. [62,63] have discovered that the low-peak-low variation of aspect ratio with aging was due to the reason that, while the diameter of precipitates has abruptly grown to a peak and then kept nearly constant, the thickness of the precipitates unvaryingly grew in a slow but stable rate. The same

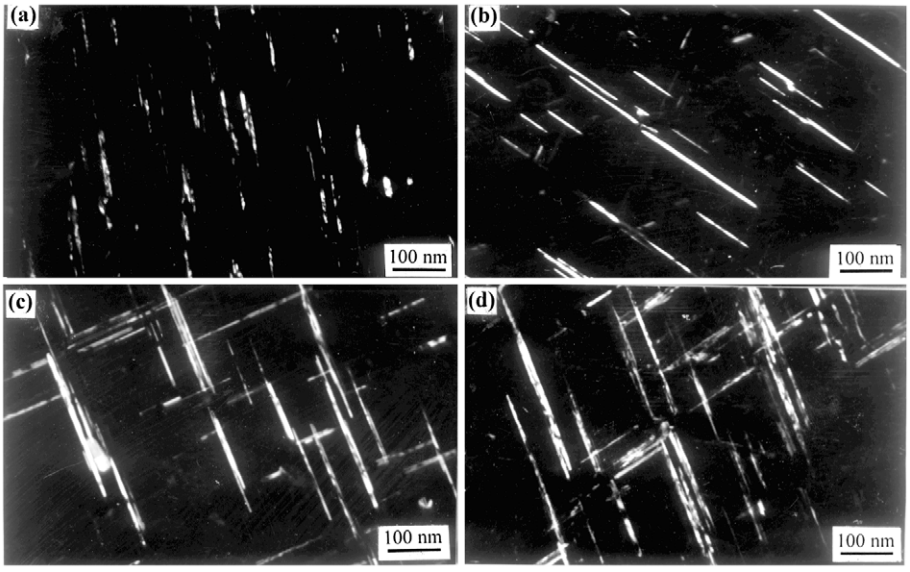

Fig. 5. TEM micrographs typically revealing the evolution of dimensions and aspect ratio of plate/disc-shaped precipitates during aging process in Al–Cu–Mg alloy aged at 513 K (a) after 0.75 h, (b) after 1.5 h, (c) after 4.0 h, (d) after 48.0 h.

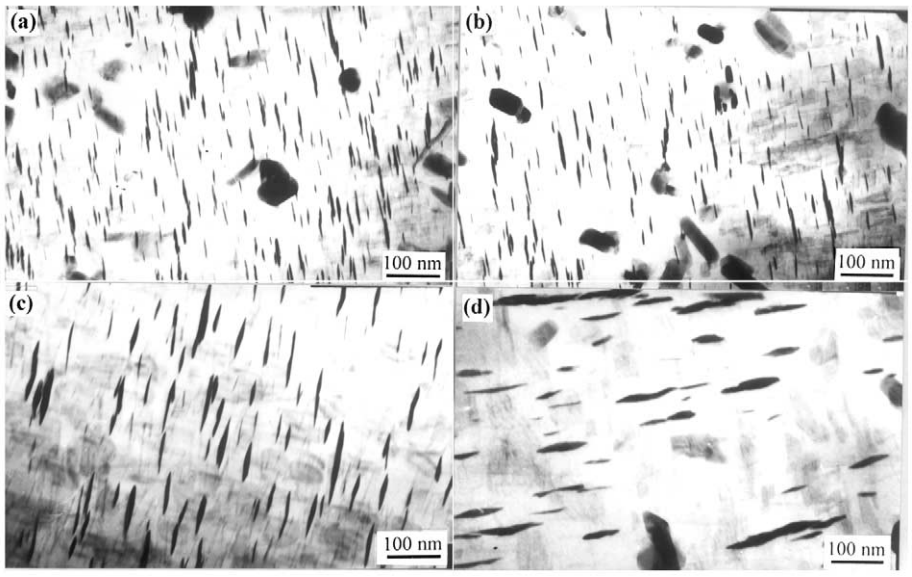

Fig. 6. TEM micrographs typically revealing the evolution of dimensions and aspect ratio of rod/needle-shaped precipitates during aging process in Al–Mg–Si alloy aged at 463 K (a) after 4.0 h, (b) after 7.0 h, (c) after 25.5 h, (d) after 48.0 h.

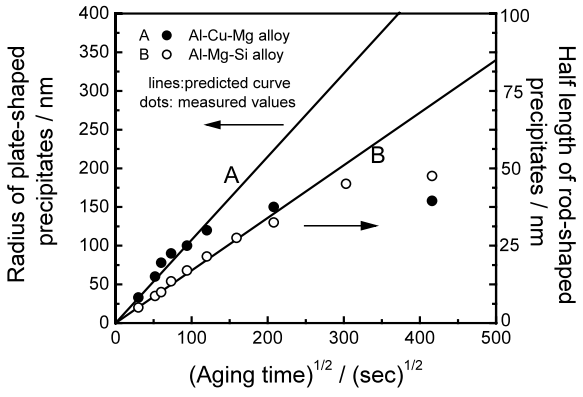

Fig. 7. Measured and predicted variation of dimension of precipitates with aging process for Al–Cu–Mg alloy aged at 513 K and Al–Mg–Si alloy aged at 463 K in present experiments.

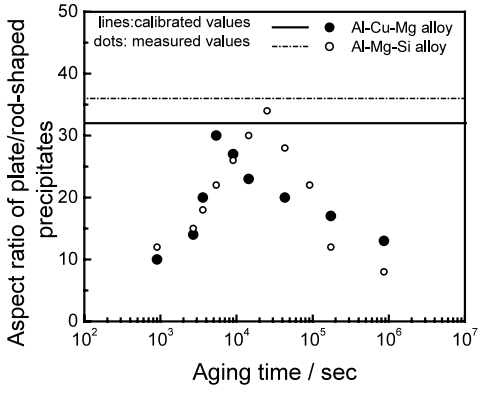

Fig. 8. Measured and calibrated variation of aspect ratio of precipitates with aging process for Al–Cu–Mg alloy aged at 513 K and Al–Mg–Si alloy aged at 463 K in present experiments.

fluctuation in comparative magnitude between the diameter and thickness of plate-shaped precipitates was also observed in aged Al–Ag alloy [33]. It seems that the phenomenon is a common regularity for precipitates and obviously it responds for the changes of aspect ratio in present experiments.

The calibrated mean aspect ratios for aged Al–Cu–Mg alloy and Al–Mg–Si alloy are drawn together in Fig. 8 for comparison with measured ones. The calculation is revealed to overrate the value during the whole aging process. But the predicted mean aspect ratios are approximately equal to the measured counterparts at the peak-aged stage, so the change of predicted mean aspect ratios can be considered as representing the change of real aspect ratios of precipitates in peak-aged aluminum alloys with different heat treatment and/or composition.

4.3. The volume fraction evolution of precipitates

Fig. 9 shows the volume fraction evolution of precipitates with aging process for the Al–Cu–Mg alloy and Al–Mg–Si alloy by both the predicted lines and measured values. Apparently, the model makes an underestimation at the underaged stage and an overestimation at the overaged stage. The overestimation at the overaged stage is because that many solute atoms are used to form constituents and dispersoids, so the solute atoms in precipitates are less than the nominal ones while in present model the two are reckoned as equal (Eq. (6)). The underestimation at the underaged stage is due to the hysteresis of simulating the precipitate density in present model. As previously defined in Section 2.1, the precipitation of strengthening phases is simulated as

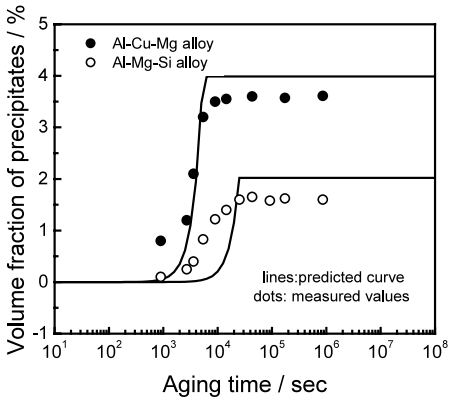

Fig. 9. Measured and predicted variation of volume fraction of precipitates with aging process for Al–Cu–Mg alloy aged at 513 K and Al–Mg–Si alloy aged at 463 K in present experiments.

being at an equal rate. In other words, at the underaged stage, the precipitation density increases in a constant rate permanently up to the moment of peak aging. In practice, however, the precipitation rate at the beginning of aging is the fastest and the rate decreases gradually down to the moment when it obtains a balance between the precipitation and the dissolution of strengthening second phases. Obviously, a certain precipitation density needed a lot of aging time to attain in the model is achieved after much less aging time in the reality, so it is displayed as the model underestimating the precipitation density at the underaged stage.

4.4. The evolution of yield strength

The measured yield strengths and predicted values of Al–Cu–Mg alloy and Al–Mg–Si alloy are depicted in Fig. 10. The predicted values are proved to broadly agree with the actual counterparts except some underestimation at the overaged stage for Al–Mg–Si alloy. This underestimation is closely associated with the overestimation in modeling the dimension of precipitates, which is due to the stagnant growth of the length

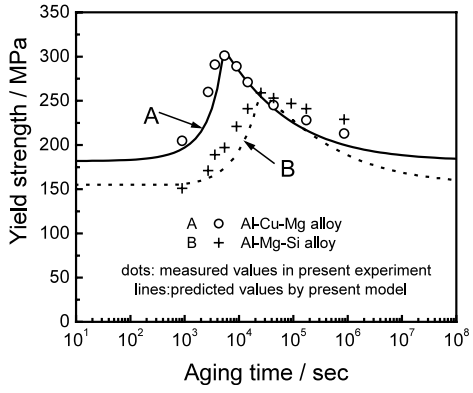

Fig. 10. Measured and predicted variation of yield strength with aging process for Al–Cu–Mg alloy aged at 513 K and Al–Mg–Si alloy aged at 463 K in present experiments.

of actual rod/needle precipitates as reflected in Fig. 7. However, the same stagnant growth of precipitates at the overaged stage is happened in Al–Cu–Mg alloy whereas only small discrepancy exists between the predicted and measured yield strengths for this alloy. Then some conflict seems to be in the explanation. In order to make certain of this difference between the two alloys and clear up the conflict in explanation, the increment of yield strength, $\Delta\sigma$, at the overaged stage is rewritten as a single function of dimension of precipitates, r or l, by regarding the product of other parameters as a constant, H

$$\Delta\sigma = \frac{H}{r}\ln\frac{0.0158r}{r_0} \tag{11}$$

Because

$$\mathrm{d}(\Delta\sigma)/\mathrm{d}r < 0 \tag{12a}$$

$$\mathrm{d}^2(\Delta\sigma)/\mathrm{d}r^2 > 0 \tag{12b}$$

the variation of $\Delta\sigma$ with r follows a line that decreases monotonously with a convex curvature just like the case in Fig. 11. Therefore the conclusion is drawn that when the r is smaller, some positive departure in r will result a enormous decrease in $\Delta\sigma$, and when the r is larger, the same positive departure in r will result a little decrease in $\Delta\sigma$. In present work, the dimensions of precipitates in Al–Mg–Si alloy are much less than those in Al–Cu–Mg, and they are both overestimated in modeling at the overaged stage. These are probably the reasons for why that the less precision was obtained in the modeled yield strength for Al–Mg–Si alloy by compared with that for Al–Cu–Mg.

5. Discussion

For the evolution of plate-shaped precipitates during aging, many researches have carried out on modeling the variation of dimensions [5–7], but very limited work has been specially done on studying the variation of aspect ratio of precipitates which hence impedes the

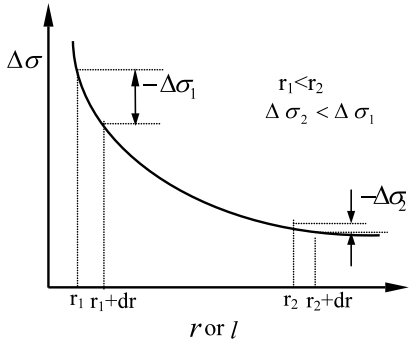

Fig. 11. The changing of increment in yield strength with dimension of precipitates at the overaged stage in this model.

analytical prediction of yield strength because the volume fracture of precipitates could not be modeled theoretically. In present work, a calibration method has been adopted to determine the aspect ratio and a series of values have been obtained for differently aged aluminum alloys of different composition. Based on these classified values together with the series of experimeantally mesured values of the present alloys, the dependences of aspect ratio of plate- and rod-shaped precipitates on aging temperature, aging time and composition could be systematically analyzed in a possibly quantitative manner and this may make some contribution to a better performance on the modeling of the yield strength.

5.1. Effect of aging temperature

In the pioneer work, an expression for quantitatively describing the aspect ratio of plate-shaped precipitates in aging has been suggested [47,48]:

$$A = A_e + \pi Bh/6\gamma \tag{13}$$

where A_e is the equilibrium aspect ratio, h and γ have been defined before, B is a function of the elastic strain, ε,

$$B = 3G\varepsilon/2(1-v) \tag{14}$$

Due to the discrepancy in crystal lattice between the precipitates and matrix on the peripheral plane, the thicker precipitates lead to more elastic strain so that a lager A is resulted according to Eq. (13) and Eq. (14). This reason seems to be responsible for the increasing of aspect ratio of precipitates in forepart of the aging process as described in Section 4.2. Along with the further thickening of precipitates, loss of coherency or semi-coherency of habit plane is taking place by the production of dislocation loops inside the precipitates and their subsequent growth through climbing to the interface [66]. The loss of coherency or semi-coherency of habit plane favors the thickening so it maybe a possible reason for the backward rebound of aspect ratio. For θ′ precipitate, the critical half-thickness, h_c of precipitates having coherent/semi-coherent plate planes is determined as [66]

$$h_c = \gamma/4G\delta^2 \tag{15}$$

where δ is the dislocation spacing after loss of coherency of ~ 0.0057. Substituting values of relevant parameters into Eq. (15) gives the critical half-thickness of θ′ precipitate being 42 nm. However, in present experiment, at the point of aspect ratio being decreasing down, the thickness of precipitates is far less than 42 nm (~ 10 nm). This means that, in currently aged Al–Cu–Mg alloy, the decisive effect for backward rebound of aspect ratio is conclusively from the stagnant growth for diameter of habit plane as well as the stable growth for non-habit plane.

5.2. Effect of aging time

In Eq. (2b), the half-thickness of plate-shaped precipitates has been related to the diffusion coefficient of solute atom in solvent, supersaturation, and aspect ratio, i.e. $h = (2/3)\sqrt{\Omega Dt/pA}$. Coupling this expression with Eq. (13) turns out the following version

$$f(A) = \sqrt{A} - \frac{A_e}{\sqrt{A}} = \frac{\pi B}{9\gamma}\sqrt{\frac{\Omega Dt}{p}} \tag{16}$$

The equation hints that, the aspect ratio of plate-shaped precipitates is influenced not only by aging time but also by diffusion coefficient and supersaturation. It is well known that the diffusion coefficient depends on aging temperatures in exponentially direct proportion and the supersaturation depends on aging temperatures in exponentially reverse proportion, so the product of diffusion coefficient with supersaturation varies with aging temperatures in a curve of saddle-shape. At lower aging temperatures, the diffusion of solute atoms is slower which results in a less value for aspect ratio, although the drive force for growth is higher. But at higher aging temperatures, the aspect ratio is still low due to a smaller drive force and the readily occurred loss of coherency or semi-coherency of habit planes. The relatively larger value for aspect ratio is obtained at intermediate aging temperature where both enough drive force for growth and enough ability for diffusion of solute atoms are contemporarily achieved. This forecast was approved in Fig. 12 which presents the variation of calibrated aspect ratios of both the Al–Cu alloys and the 6061 alloys in Section 2 with aging temperatures. For the Al–Cu alloys of Hardy [34], the derived aging temperature for getting maximum mean

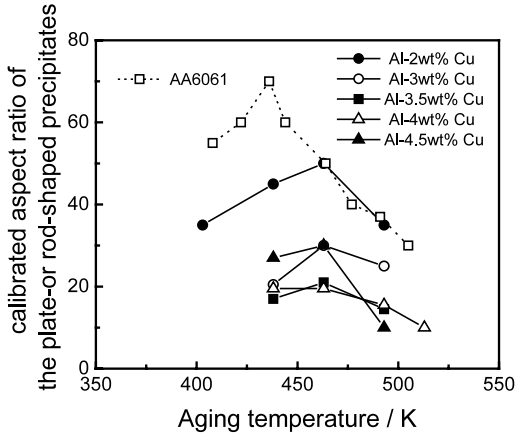

Fig. 12. Dependence of calibrated aspect ratio of plate- or rod-shaped precipitates on aging temperatures for both the Al–Cu binary alloys and the AA6061.

aspect ratio is 463 K, and for the 6061 alloy of Anderson [49] it is 436 K. Aged at other temperatures deviating from the two ones, both right and left side, all cause the reduction in mean aspect ratio for the two alloys, separately. Some others' works confirm this conclusion by observing facts that the aspect ratio of plate-shaped precipitates in aged Al–4 wt.% Cu decreased gradually with aging temperature elevated from 473 to 573K [12,62].

5.3. Effect of composition

The composition of aluminum alloys is also a significant factor in controlling the aspect ratio of precipitates. It can be inferred from Eq. (16) that higher nominal content of solute in solution will bring about more enough supersaturation and concomitant larger aspect ratio. But from Fig. 12 the 2 wt.% Cu-containing alloy is shown to possess the largest aspect ratio and subsequently the aspect ratio is decreasing with content increasing until more than 4 wt.% Cu being up to. This may be ascribed to the ability for nucleation and growth of precipitates. When the nominal content of solute is lower, like 2 wt.% Cu, the drive force for nucleating precipitates is weaker, so less density is come out for precipitates and the excess solute atoms are adequate to meet the need for unlimited extension of habit plane of precipitates. As the nominal content being added, more strengthening phases are precipitated and the diffusion fields for growth of precipitates are ready to overlap which limits the free extension of precipitates and leads to a less aspect ratio. However, when the nominal content is enhanced to a very much level, like 4.5 wt.% Cu, affluent solute atoms ensure the differently oriented precipitates growing enough to impinge or be highly adjacent. At this time, a rapid transfer of copper atoms between contacted or adjacent precipitates could take place in a manner as illustrated in [48]. The easy-diffusion path promotes the spreading of plate plane of precipitates then help the aspect ratio to increase again.

6. Summary and conclusions

In this paper we have modified a simple model for predicting the yield strength of plate or needle-shaped-precipitates containing Al aluminum alloys by considering the strengthening of the precipitates coupled with the whole evolution process, i.e. nucleation, growth and coarsening of the precipitates, with all the involved parameters having transparent physical meanings. After verifying the validity of the modified model by both previously measured values of three kinds of heat-treatable aluminum alloys and the present experiments, the conclusions are drawn as follows:

(1) This model is suitable for predicting the yield strength of both plate-shaped precipitates and rod/needle-shaped precipitates containing aluminum alloys during the whole aging process by simulated values being agreeable with the measured counterparts.

(2) At the underaged stage and the forepart of overaged stage, the modeled radius (half-lengths) of plate-shaped (rod/needle-shaped) precipitates fit well with the actual ones indicating that the growth of precipitates following the $t^{1/2}$ law, and the growth rate of thicker dimension is much larger than that of thinner dimension indicating the growth of precipitates being controlled by interface diffusion.

(3) The aspect ratio of plate-shaped (rod/needle-shaped) precipitates experimentally varies with aging process in a low-to-peak-to-low manner. The same trend is calibrated in the changing of aspect ratio with aging temperature while the nominal composition affects the aspect ratio in an inverse fashion, i.e. high-to-bottom-to-high.

Acknowledgements

The financial auspice from State Key Project of Fundamental Research of China (Grant NO.G1999064909) is sincerely acknowledged. The authors also wish to express their special thanks for the support from the National Natural Science Foundation of China and the Outstanding Young Investigator Grant of China. Valuable comments and kindly suggestions from the reviewer are sincerely appreciated too.

References

[1] J.W. Cahn, J.E. Hilliard, J. Chem. Phys. 28 (1958) 258.
[2] H.I. Aaronson, K.R. Kinsman, K.C. Russell, Scripta Metall. 4 (1970) 101.
[3] J.W. Cahn, Acta Metall. 10 (1962) 179.
[4] J.D. Eshelby, Proc. R. Soc. A241 (1957) 376.
[5] F.S. Ham, J. Phys. Chem. Solids 6 (1958) 335.
[6] F.S. Ham, J. Appl. Phys. 17 (1959) 137.
[7] G. Horvay, J.W. Cahn, Acta Metall. 9 (1961) 695.
[8] J.S. Langer, A.J. Schwarz, Phys. Rev. A21 (1980) 948.
[9] H. Wendt, P. Haasen, Acta Metall. 31 (1983) 1946.
[10] K. Abbott, C.W. Haworth, Acta Metall. 21 (1973) 951.
[11] R. Sankaran, C. Laird, Acta Metall. 22 (1974) 957.
[12] Y.H. Chen, R.D. Doherty, Scripta Metall. 11 (1977) 725.
[13] H.R. Shercliff, M.F. Ashby, Acta Metall. Mater. 38 (1990) 1789.
[14] H.R. Shercliff, M.F. Ashby, Acta Metall. Mater. 38 (1990) 1803.
[15] A. Deschamps, Y. Brechet, Acta Mater. 47 (1999) 281.
[16] A. Deschamps, Y. Brechet, Acta Mater. 47 (1999) 293.
[17] Ø. Grong, O.R. Myhr, Acta Mater. 48 (2000) 445.
[18] O.R. Myhr, Ø. Grong, Acta Mater. 48 (2000) 1605.
[19] Ø. Grong, H.R. Shercliff, Prog. Mater. Sci. 47 (2002) 163.
[20] B. Reppich, in: R.W. Cahn, P. Haasen, E.J. Krammer (Eds.), Material Science and Technology, vol. 6, VCH, Weinheim, 1993, p. 311.
[21] P. Merle, F. Fouquet, J. Merlin, Mater. Sci. Eng. 50 (1981) 215.

[22] P. Merle, F. Fouquet, J. Merlin, in: P. Haasen, V. Gerold, G. Kostorz (Eds.), Strength of Metals and Alloys, Pergamon Press, 1979, p. 657.
[23] P.M. Kelly, Scripta Metall. 6 (1972) 647.
[24] J.F. Nie, B.C. Muddle, I.J. Polmear, Mater. Sci. Forum 217–222 (1996) 1257.
[25] A.W. Zhu, A. Csontos, E.A. Starke, Jr., Acta Mater. 47 (1999) 1713.
[26] A.W. Zhu, E.A. Starke, Jr., Acta Mater. 47 (1999) 3263.
[27] A.K. Jena, M.C. Chaturvedi, Phase Transformation in Materials, Prentice-Hall Press, New Jersey, 1992, p. 151.
[28] K.C. Russell, Adv. Colloid Interface Sci. 13 (1980) 205.
[29] D.A. Porter, K.E. Easterling, Phase Transformation in Metals and Alloys, Van Nostrand-Reinhold, Workingham, 1992, p. 285.
[30] R.D. Doherty, in: R.W. Cahn, P. Haasen (Eds.), Physical Metallurgy, Elsevier, NewYork, 1983, p. 933.
[31] K.R. Kinsman, H.I. Aaronson, C. Laird, Acta Metall. Mater. 15 (1967) 1244.
[32] M. Ferrante, R.D. Doherty, Acta Metall. 27 (1979) 1603.
[33] R. Wagner, R. Kampmann, in: R.W. Cahn, P. Haasen, E.J. Krammer (Eds.), Material Science and Technology, vol. 5, VCH, Weinheim, 1991, p. 246.
[34] H.K. Hardy, J. Ins. Metals 79 (1951) 321.
[35] E. Hornbogen, Aluminium 43 (1967) 115.
[36] A.W. Zhu, E.A. Starke, Jr., Acta Mater. 49 (2001) 3063.
[37] F. King, Aluminum and its Alloys, Ellis Horwood Limited, Chichester, 1987, p. 22.
[38] Metals Handbook (Ninth Edition), Vol. 2, Properties and Selection: Nonferrous Alloys and Pure Metals, American Society for Metals, 1979.
[39] G. Lorimer, in: K.C. Russell, H.I. Aaronson (Eds.), Precipitation in solid, The Metallurgical Society, 1978, p. 87.
[40] R.A. Swalin, Thermodynamics of Solids, Wiley, NewYork, 1962.
[41] C. Laird, H.I. Aaronson, Acta Metall. 14 (1966) 171.
[42] M. Beyeler, M. Maurice, R. Seguin, Mem. Sci. Rev. Metall. 67 (1970) 295.
[43] H. Hargarter, M.T. Lyttle, E.A. Starke, Jr., Mater. Sci. Eng. A 257 (1998) 87.
[44] P.M. Kelly, Scripta Metall. 6 (1972) 647.
[45] H.I. Aaronson, J.B. Clark, C. Laird, Metal Sci. J. 2 (1968) 155.
[46] R.D. Doherty, M. Ferrante, Y.H. Chen, Metal Sci. J. 12 (1978) 885.
[47] J.D. Boyd, R.B. Nicholson, Acta Metall. 19 (1971) 1101.
[48] J.D. Boyd, R.B. Nicholson, Acta Metall. 19 (1971) 1379.
[49] W.A. Anderson, Precipitation from Solid Solution, American Society of Metals, Metals Park, Ohio, 1959.
[50] O.R. Myhr, Ø. Grong, S.J. Anderson, Acta Mater. 49 (2001) 65.
[51] D.H. Bratland, Ø. Grong, H. Shercliff, O.R. Myhr, S. Tjøtta, Acta Mater. 45 (1997) 1.
[52] Ø. Grong, Metallurgical Modelling of Welding, second ed., The Institute of Materials, London, 1997.
[53] C.P. Blackenship, E.A. Starke, Jr., E. Hornbogen, in: J.C.M. Li (Ed.), Microstructure and Properties of Materials, World Scientific Publishing Corp. Ltd, 1996, p. 45.
[54] S.J. Andersen, H.W. Zandbergen, J. Jansen, C. Træholt, U. Tundal, O. Reiso, Acta Mater. 46 (1998) 3283.
[55] X.Z. Li, V. Hansen, J. Gjønnes, L.R. Wallenberg, Acta Mater. 47 (1999) 2651.
[56] A.M. Ei Sheikh, in: J.P. McQueen, Bailon, J.I. Dickson, J.J. Jonas, M.G. Akben (Eds.), Strength of Metals and Alloys, Pergamon Press, 1986, p. 483.
[57] A. Deschamps, Y. Bréchet, Mater. Sci. Eng. A 251 (1998) 200.
[58] J.M.G. Crompton, R.M. Waghorne, C.B. Brook, Br. J. Appl. Phys. 16 (1966) 277.
[59] D.L. Gilmore, E.A. Starke, Jr., Metall. Mater. Trans. 28A (1997) 1399.
[60] J.W. Edington, Practical Electron Microscopy in Materials Science, Van Nostrand Reinhold Company, London, 1976, p. 207.
[61] L.F. Mondolfo, Aluminum Alloys: Structure and Properties, Butterworths, 1976.
[62] P. Merle, F. Fouquet, Acta Mater. 29 (1981) 1919.
[63] P. Merle, F. Fouquet, Acta Mater. 29 (1981) 1929.
[64] R. Sankaran, C. Laird, Scripta Metall. 11 (1977) 383.
[65] R. Sankaran, C. Laird, Scripta Metall. 12 (1978) 877.
[66] G.C. Weatherly, R.B. Nicholson, Phil. Mag. 17 (1968) 801.